Preprints (www.preprints.org) | NOT PEER-REVIEWED | Posted: 30 April 2018 doi:10.20944/preprints201804.0386.v1

Article

Debonding Detection of Steel-UHPC Composite Slab Using PZT Technology and Clustering Algorithm

Banfu Yan[1], Qiqi Zou[2], You Dong[3,*], and Xudong Shao[4]

[1] Associate Professor, College of Civil Engineering, Hunan University. Yuelushan, Changsha, 410082, Hunan, China; yanbanfu@hnu.edu.cn;
[2] Ph.D. Candidate, College of Civil Engineering, Hunan University, Yuelushan, Changsha, 410082, Hunan, China; zouqiqi@hnu.edu.cn;
[3] Assistant Professor, Department of Civil and Environmental Engineering, The Hong Kong Polytechnic University, Hong Kong, China, you.dong@polyu.edu.hk, *: corresponding author;
[4] Professor, College of Civil Engineering, Hunan University. Yuelushan, Changsha, 410082, Hunan, China. shaoxd@hnu.edu.cn
* Correspondence: you.dong@polyu.edu.hk; Tel.: +852-3400-8818

Abstract: A lightweight composite bridge deck system composed of steel orthotropic deck stiffened with thin Ultra-High Performance Concrete (UHPC) layer is developed to eliminate fatigue cracks in orthotropic steel decks. During the construction and operation period of the bridge, the debonding between the steel deck and the UHPC layer may introduce the several issues, such as crack-induced water invasion and distinct reduction of the shear resistance. In the study, an effective and novel non-destructive interface condition monitoring approach using piezoelectric lead zirconate titanate (PZT)-based technologies is proposed to detect interfacial delamination between steel deck and UHPC layer. Experimental tests are performed on several steel-UHPC composite slabs and a conventional steel-concrete composite slab. The thin styrofoam sheets with different sizes and thicknesses are set on different locations of the steel deck as the artificial debondings. The PZT ceramic patches are bonded on the surfaces of the steel deck and UHPC layer as the actuators/sensors. An improved PSO (Particle Swarm Optimization)-K-means clustering algorithms is proposed to obtain the debonding patterns based on the feature data set. The laboratory tests demonstrate that the proposed approach provides an effective and accurate way to detect interfacial debonding of steel-UHPC composite slab.

Keywords: Steel-UHPC, Composite slab, Debonding detection, PZT technology, Clustering algorithm

---

1. Introduction

The lightweight steel-UHPC composite bridge deck system composed of steel deck and thin reinforced UHPC layer through stud shear connectors is an effective way to eliminate bridge defects, such as preventing wearing and reducing fatigue cracking of the orthotropic steel deck [1-4]. In practice, however, the construction of this innovative structure is very challenging due to several reasons. First, the thickness of UHPC layer in the composite bridge is 35 - 50mm, which requires a specific caring and high-temperature steam treatment. Second, the steel-fiber volume ratio in the structure is up to 3.5%, which could cause larger clusters. Third, the high-temperature steam treatment can cause the debonding between the steel and UHPC layer. Last but not least, the performance of the steel-UHPC composite deck system may degrade due to the possible vehicle overloading and high-temperature action during operation. Hence, the debonding between the steel deck and the UHPC layer may introduce the risks such as cracking-induced water invasion and distinct reduction of the shear resistance of the bridge deck system. Thus, it is of vital importance to effectively detect the interface debonding of steel-UHPC deck system.

The piezoelectric ceramic patches (PZT) sensor made of piezoelectric ceramics with both positive and negative piezoelectric effects can be used simultaneously as actuator and sensor. Due to its lightweight characteristic, the PZT sensor can be installed on the surface of an existing structure or embedded into the newly-built structure for damage detection purpose. Within the application of civil engineering, the PZT sensor has been demonstrated to be particularly advantageous due to its unique features, such as passive sensing, high-sensitivity, low cost, quick response, among others. In recent years, the PZT-based approach has been broadly recognized as one of the most promising non-destructive evaluation method for local damage identification [5-6]. The PZT-based damage identification methods can be classified into two major groups: the impedance-based method and the vibration-characteristic-based wave propagation method.

The impedance method intends to evaluate the status of a structure through the mechanic-electric coupling between the piezoelectric material and the structure. The impedance of PZT material can be derived from an ideal one-dimensional model. When the structure is damaged, its local stiffness decreases, leading to the impedance change of the structure. Thus, the structural damage detection and health monitoring can be realized through monitoring the impedance change of PZT installed on the surface or inside of a structure. In past decades, many studies have been conducted on applying the PZT impedance method for structural damage detection and health monitoring (e.g., [7-14]). Sun et al. [7] proposed a frequency domain impedance-signature-based technique for health monitoring of an assembled truss structure and used PZT as integrated sensor-actuators; Liang et al. [8] developed a coupled electro-mechanical analysis of piezoelectric ceramic actuators integrated in mechanical systems to determine the power consumption and energy transfer in the electro-mechanical systems; Yang et al. [9] conducted an experimental study on local damage detection of beams and plates by using the PZT and demonstrated that both the location and extent of damage can be simultaneously identified; Coverlet et al. [10] developed a new method of impact location in composite materials using piezoceramic sensors; Karayannis et al. [11] assessed the damage of concrete reinforcing bars using bonded piezoelectric transducers; Xu et al. [12] investigated the structural crack damage using the impedance spectra of the PZT sensor, and presented a scalar damage metric based on the impedance spectra of the PZT piezoelectric sensor; Sevillano et al. [13] proposed an innovative hierarchical clustering analysis in order not only to obtain a set of clusters based on damage patterns found in experimental data obtained with PZT sensors, but also to achieve a graphical representation of this information; Liang et al. [14] detected the bond-slip occurrence of the concrete-encased composite structure using the electro-mechanical impedance technique.

With respect to the vibration-characteristic-based wave propagation method, the piezoelectric actuators attached on the surface or embedded in the structure would generate stress wave under external excitation, which can be received by the piezoelectric sensors. Vibration features extracted from the acquired stress wave, such as the changes of signal strength, arrival time, and transfer function before and after the introduction of damage, are used for structural damage detection. Wang et al. [15] proposed an active diagnostic technique for identifying impact damage in composite plates. This technique used a built-in network of piezoelectric actuators and sensors to generate and receive propagating stress waves over a wide range of frequencies. Chang et al. [16] developed a diagnostic technique based on a built-in network of piezoelectric actuators and sensors for detecting the location and size of anomaly in isotropic plates. Wang et al. [17] proposed an active diagnostic system to detect embedded damage in fiber-reinforced composites and steel-reinforced concrete. Song et al. [18] used piezoceramic transducers for damage detection of a reinforced concrete bridge bent-cap. During the experimental test, one embedded piezoceramic patch is used as an actuator to generate high frequency waves, and the other piezoceramic patch works as sensors to detect the propagating waves. A damage index was proposed on the basis of the wavelet packet analysis. Lim et al. [19] performed a series of experimental studies to investigate the application of the wave propagation (WP) technique in concrete curing and strength development monitoring. Ye et al. [20] investigated the propagation of ultrasonic waves in rebar-reinforced concrete beams for the purpose of damage detection. Experimental test demonstrated that the surface-attached PZT disks were able to detect the change in material properties due to the existence of cracking. Xu et al. [21] proposed an active

Preprints (www.preprints.org) | NOT PEER-REVIEWED | Posted: 30 April 2018 doi:10.20944/preprints201804.0386.v1

interface condition monitoring approach for concrete-filled steel tube (CFST) by the use of functional smart aggregates (SAs) embedded in concrete as actuator and PZT patches bonded on the surface of the steel tube as sensors.

This study aims to develop an integrated approach to detect the interfacial debonding of steel-UHPC composite slab. Both impedance analysis and wave propagation method are employed to extract the debonding features of the steel-UHPC composite slab with different preset debonding defects. Additionally, an improved PSO-K-means clustering algorithm is proposed to extract the clustering centers of the feature data set, and the Mahalanobis distance is used to distinguish the debonding degree of the deck system. The proposed methodology is validated through experimental tests on two steel-UHPC composite slabs and a steel-NSC composite slab with different artificial debonding damages.

2. Experimental work

2.1 Specimen and sensor installation

Three specimens termed as A-type steel-UHPC composite slab with different preset debonding sizes, B-type steel-UHPC composite slab, and C-type conventional steel-concrete composite slab with different debonding thickness values are prepared with the same dimension of 800mm (length) × 300mm (width) × 64mm (height). As shown in Figure 1, the specimen consists of a bottom steel plate with a thickness of 14 mm and a 50 mm-thick UHPC. The steel of the bottom plate is with a yield strength of 345MPa. The UHPC is reinforced by HRB400 rebar with a diameter of 10 mm and spaced at 50mm interval in both longitudinal and transverse directions. Before casting the 50mm-thick UHPC overlay, the styrofoam sheets with different sizes and thicknesses were embedded in steel-UHPC interfaces to simulate the interfacial debonding and water invading, as indicated in Figure 1.

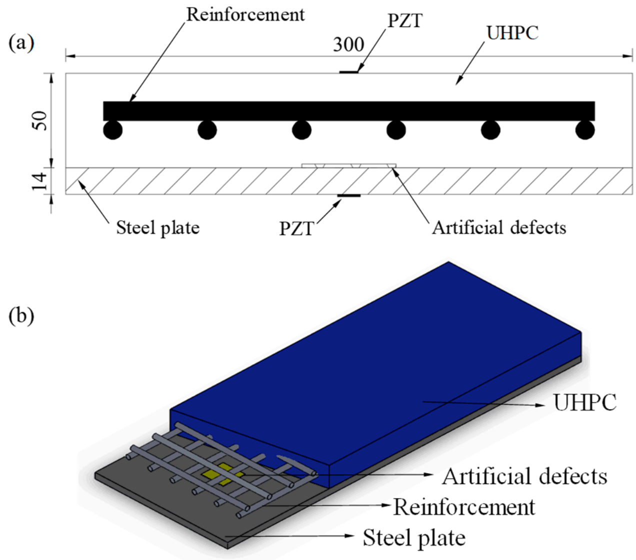

Figure 1. (a) 2-dimentional and (b) 3-dimental investigated system

As shown in Figure 2, the A-type plate is configured with 5 pieces of tyrofoam sheet as debonding defects. The effect of debonding size on the identification accuracy was investigated. The 5 sheets ranging from 10mm × 10mm (D5) to 50mm × 50mm (D1) in dimension and 2mm in identical thickness are uniformly distributed along the length of the specimen with a uniform distance of 150mm. Moreover, 5 pair of PZT patches with the locations (D1 – D5) identical to those of the sheets and a pair of PZT patches with intact bonding interface (D0) were bonded symmetrically on bottom side of steel plate (PZT06 – PZT5) and top surface of UHPC (PZT6 – PZT11).

Preprints (www.preprints.org) | NOT PEER-REVIEWED | Posted: 30 April 2018 doi:10.20944/preprints201804.0386.v1

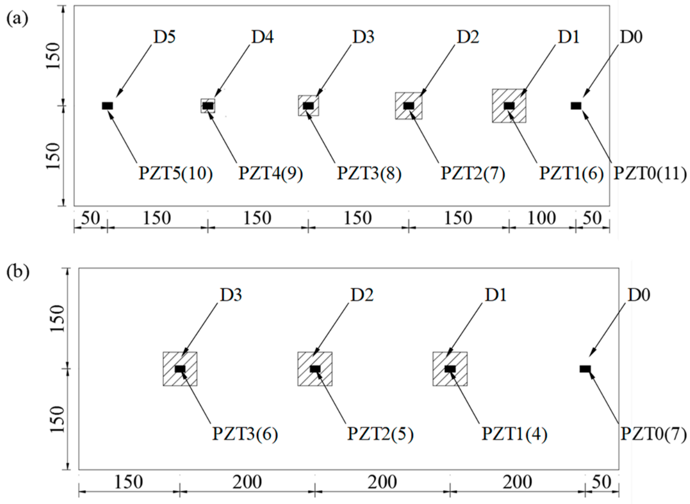

Figure 2. Defects and testing points of (a) A-tyep and (b) B-type

To investigate the effect of debonding thickness on the identification accuracy, the B-type steel-UHPC plate, designed to be having the same dimension and reinforcement as A-type plate, is embedded with 3 pieces of 50mm × 50mm tyrofoam sheets with the thickness of 1mm, 2mm, and 3mm as indicated in Figure 2(b). The number in brackets (Figure 2(b)) indicates the PZT patches attached onto the top surface of UHPC. Note that the material type of overlay has an effect on the PZT sensor signature. To investigate the difference of PZT sensor signatures at the steel-UHPC and steel-NSC composite structures, as well as the effectiveness of the damage detection method, a C-type plate is constructed with the same dimension, defects and sensor placement as the B-type plate except that the overlay is composed of normal concrete.

2.2 Instrumental setup

2.2.1. Impedance method

The instrumental setup is shown in Figure 3(a). The impedance analyzer (Agilent HP4192A) is employed to measure the admittance signatures of the PZT sensor on the surface of steel plate. The PZT piezoelectric sensor is excited by alternating voltage with constant amplitude at preset frequency bands from the impedance analyzer. The impedance signature of the electromechanical coupling system composed of PZT patch, steel plate, and UHPC overlay is transmitted and stored by the laptop via GPIB connection. Features sensitive to damage degree are extracted from the electromechanical coupling impedance-frequency curves of the PZT sensors at the different preset damage locations. The extracted features are then employed to identify and quantify the debonding damages in the steel-UHPC composite structure. Table 1 shows the main properties of the high-sensitivity PZT sensor with a dimension of 15mm (length) × 10mm (width) × 0.3mm (thickness).

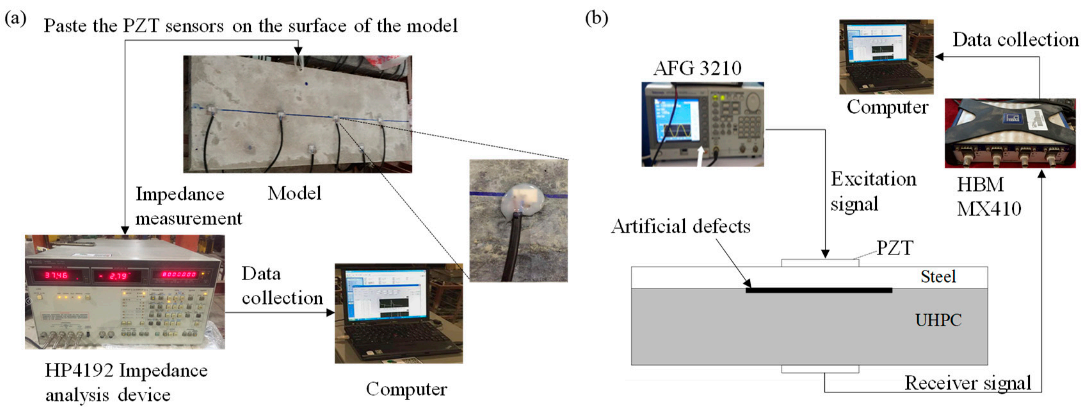

Figure 3. Testing system of (a) impedance method and (b) wave propagation method

Preprints (www.preprints.org) | NOT PEER-REVIEWED | Posted: 30 April 2018 doi:10.20944/preprints201804.0386.v1

Table 1. Properties of the PZT sensors.

Properties	Values	Properties	Values
Piezoelectric strain factor d33 (10-12C/N)	450	Curie point (℃)	310
Relative dielectric constant ε33/ε0	1800	Dielectric loss (%)	1.5
Electromechanical coupling factor k33	0.71	Density (g/cm3)	7.6
Mechanical quality factor Q	65		

2.2.2. Wave propagation method

The wave propagation measurement system consists of PZT sensors, arbitrary waveform/function generator (Tektronix AFG3210), MX410 dynamic signal amplifier (HBM), testing specimen and laptop, as indicated in Figure 3(b). Sweep sinusoidal signal with a preset frequency bands generated by AFG3210 waveform/function generator is imposed on the PZT transducer bonded on the bottom surface of steel plate. The stress wave propagates through the steel-UHPC composite structure with preset debonding defects and was acquired individually by the PZT sensor bonded on the top surface of UHPC overlay through a high-speed data acquisition system MX410 dynamic signal amplifier. The debonding defects are then identified and quantified through analyzing the variation of the vibration parameters, such as signature amplitude, frequency spectral, and energy distribution, etc.

2.3. Testing scenarios

The PZT impedance technique is employed to measure the high frequency local impedance, which is sensitive to local damage of the structure. The sensitivity parameters related to the structural damage detection depend on many factors. Table 2 shows the testing scenarios of the PZT impedance-based identification techniques. The three-type specimens are tested under different scenarios, such as frequency bands of the impedance analyzer, location of PZT sensor, material type of overlay (e.g., UHPC and NSC), thickness and size of preset debonding defect. The sensitive features are then extracted from the impedance-frequency curves of the PZT sensors bonded at the surface of composite structure for further analysis.

Table 2. Testing scenarios associated with impedance method

Testing parameters	Testing model	Measurement frequencies (kHz)
Different measurement frequencies	B	100~12000
Relative location of different testing points	B	6000~8000, 10000~12000
Different materials (i.e., UHPC and NSC)	B, C	6000~8000
Different defect Thickness	B	6000~8000, 10000~12000
Different defect Size	A	6000~8000, 10000~12000

In terms of wave propagation method, the propagation of stress wave in the structure can be affected by three main factors, i.e., excitation voltage amplitude, frequency and propagation media (i.e., UHPC and NSC). The effects of factors on the damage identification are investigated herein. The PZT actuators besides the steel plate are excited by the preset damage location (e.g., separation thickness and quantity). The PZT sensors located on the surface of UHPC receive the wave signal. Sensitive features extracted from the signal are employed to identify and quantify the damage in the structure. The testing scenarios for the wave propagation method are indicated in Table 3.

Table 3. Testing scenarios associated with wave Propagation method

Testing parameters	Testing model	Excitation signal
Different amplitude of excitation signal	B	1~5V (10kHz)
Different frequency of excitation signal	B	1~30kHz (5V)
Different materials (i.e., UHPC and NSC)	B, C	10kHz (5V)
Different defect Thickness	B	10kHz, 15kHz (5V)
Different defect Size	A	10kHz, 15kHz (5V)

3. Experimental results

3.1 Impedance method

3.1.1. Different Frequency bands

Impedance-based damage detection depends on the selection of frequencies. The frequency with the larger range is first selected through a larger interval scanning. Among the roughly selected frequencies, the frequencies with obvious features, e.g., wide fluctuation, obvious wave peaks and troughs, and trend change, are scanned again at a smaller interval. This procedure is iteratively applied until a proper frequency range is obtained. In this study, two frequency ranges, i.e., 6000 - 8000 kHz and 10000 - 12000 kHz are selected. Figure 4 shows the impedance curves of B-type plate. It is observed that the impedance-frequency curves show the similar trends, but their peaks indicate significant difference. The larger debonding thickness produces higher impedance peak and average values.

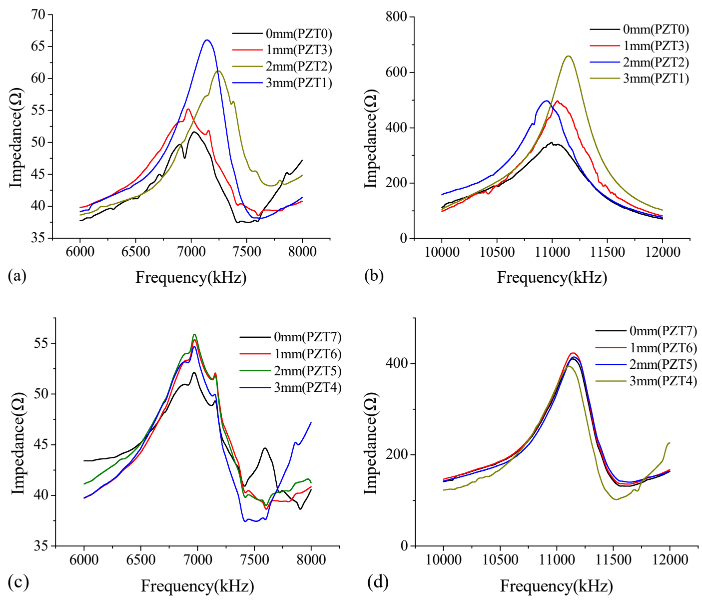

Figure 4. Impedance curve of the PZT sensors attached on the steel surface at the B-type plate (a) 6000~8000kHz; (b) 10000~12000kHz; Impedance curve of the PZT sensors attached on the UHPC surface at the B-type plate (c) 6000~8000kHz; and (d) 10000~12000kHz.

3.1.2. Relative locations of testing points

Figure 5 shows the impedance-frequency curves for the PZT in B-type UHPC plate. In the same frequency range, the curves show the similar trend, but the difference among the impedance curves is insignificant for the PZT sensors attached to the concrete surface. Compared with Figure 4, the significant fluctuation is observed for the PZT sensors attached to the steel surface, thus, implying more sensitive to the local separation. This attributes to the fact that the impedance-based method is a type of local measurement techniques. The thickness of the steel plate is far smaller than that of concrete plate; thus, the PZT sensor on the steel surface is much closer to the damage zone.

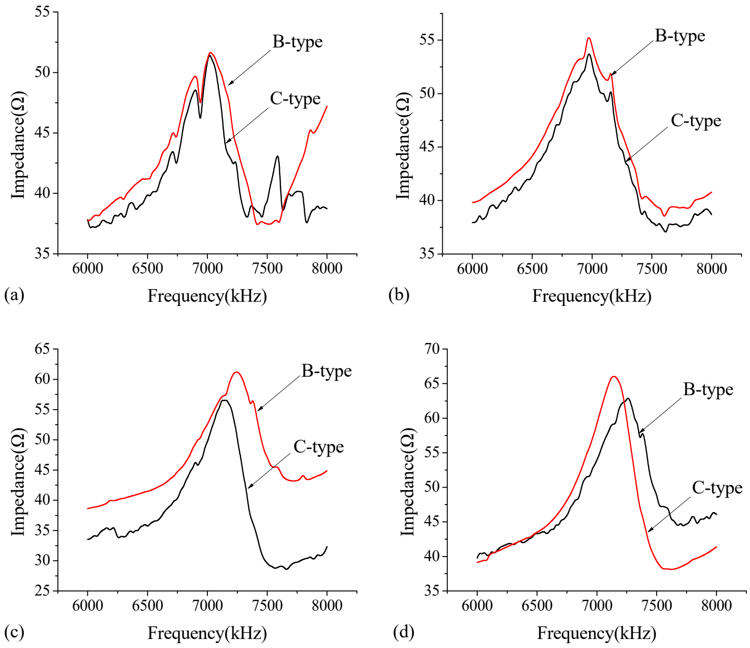

Figure 5. Impedance curve of the PZT sensors attached on the steel surface at the B-type and C-type plate (a) 0 mm defect thickness; (b) 1 mm defect thickness; (c) 2 mm defect thickness; and (d) 3 mm defect thickness.

3.1.3. Steel-UHPC vs Steel-NSC

Figure 5 shows the impedance curves for steel-NSC composite plat (C-type) under different defect thickness. Additionally, its comparison to B-type plat was also indicated in this figure. As indicated, the trends of the impedance curves for both C-type and B-type plats are almost the same, but the impedance of the former is slightly smaller. The separation of two curves are obvious, implying that the selected frequency range is feasible for damage detection of the investigated two types of plates. The impedance curves of B and C-type plates nearly coincides when the damage thickness is less than 1mm, while the separation of two curves is significant when the damage thickness is over 2 mm, implying that the damage turns to be more significant and the materials play a key role on the impedance curves. It is also observed that the peak of B-type plate is generally larger than that of C-type plate. This implies that given the composite plate made of cement materials, either plain concrete or UHPC, the higher the strength of concrete plate is, the larger the peak of PZT impedance is. This result has demonstrated that the impedance method is effective in identifying the damage in the both steel-UHPC and steel -NSC.

3.1.4. Debonding degree

In this study, the root-mean-square deviation (RMSD) is employed to quantify the debonding degree of impedance curves, expressed as follows:

$$RMSD = \sqrt{\frac{\sum_{1}^{N}(Z_i^1 - Z_i^0)^2}{\sum_{1}^{N}(Z_i^0)^2}} \times 100\% \tag{1}$$

where N is the number of data points obtained from testing; Z_i^0 is the real part of impedance at the healthy condition; and Z_i^1 is the real part of impedance at the damage condition.

Figures 6 shows the RMSD values of A-type plates at two frequency ranges of 6000 - 8000 kHz and 10000 - 12000kHz. It is observed that, as the debonding area increases, the RMSD value in the frequency range of 6000 - 8000kHz varies slightly; thus, this range is not sensitive to the damage. When the debonding area reaches up to 50mm × 50mm, the damage index increases significantly given the existence of damage. In the frequency range of 10000 - 12000kHz, the RMSD value is relatively larger as the debonding area increases, which means that this range is sensitive to the debonding degree. However, the RMSD value becomes relatively large only when the debonding area reaches up to 30mm × 30mm.

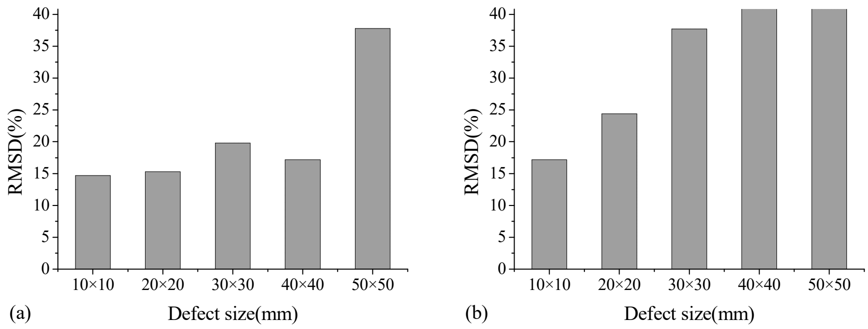

Figure 6. RMSD values of A-type plate (a) 6000~8000kHz and (b) 10000~12000kHz

3.2 Wave propagation method

3.2.1. Amplitude of excitation signal

It has been well recognized that the response of PZT material is proportional to the applied external force (F) and electric field strength (E). The linearity of the PZT sensor is employed to investigate the linear relationship of the signal inputs and outputs. Figure 7(a) shows the linear relationship of the signal amplitude vs excitation voltage amplitude of the healthy location for B-type plates. It is observed that the linear relationship in this case is significant, i.e., the amplitude of signal increase as the amplitude of excitation voltage increases. This has demonstrated that the linearity of wave propagation based testing system for the design model is acceptable and the data acquisition from the testing system is reliable.

3.2.2. Excitation voltage frequency

Figure 7(b) shows the relationship between the receiver signal amplitude and the excitation voltage frequency for B-type plate. As indicated, the wave propagation is affected significantly by the excitation signal frequencies. When the excitation signal frequency is below 5kHz or above 15kHz, the amplitude difference of various damage scenarios is insignificant; thus, the damage cannot be detected effectively. When the excitation frequency falls between 5 and 15kHz, the difference of the receiver signal amplitudes at different damage cases is obvious. In this study, the frequencies of 10 kHz and 15 kHz are used for testing.

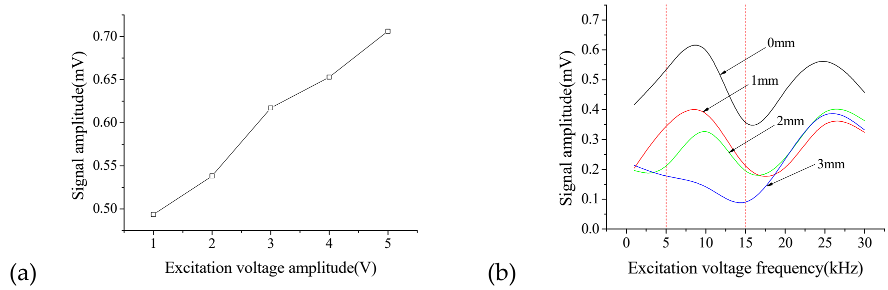

Preprints (www.preprints.org) | NOT PEER-REVIEWED | Posted: 30 April 2018 doi:10.20944/preprints201804.0386.v1

Figure 7. (a) Linear relationship of the signal amplitude v.s. excitation voltage amplitude of the healthy location for B-type plates and (b) receiver signal amplitude vs the excitation voltage frequency for B-type plates.

3.2.3. Steel-UHPC vs Steel-NSC

The receiver signal for B-type steel-UHPC and C-type steel-NSC is shown in Figure 8. As indicated, the wave trends of two types plates are similar, while the signal amplitude of B-type plate is larger than that of C-type plate. This is attributed to the fact that the B-type UHPC plate has no coarse aggregate. In comparison to the plain concrete, the UHPC has the less energy dissipation. The amplitude of the curves in time-domain has significant variation for both B and C-type plates. Thus, the wave propagation method is effective in detecting the damage for both steel-UHPC and steel-NSC composite plates.

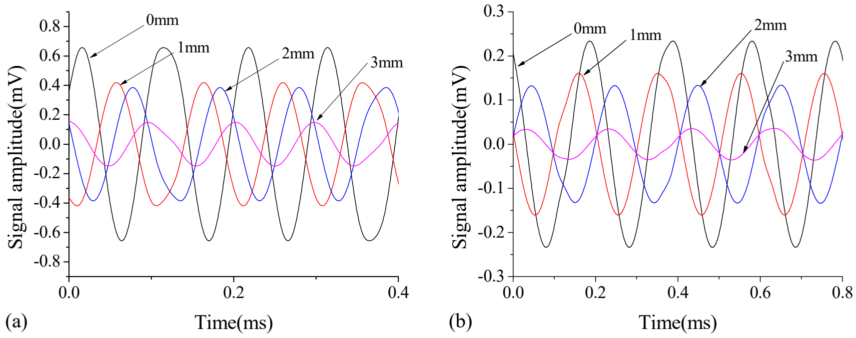

Figure 8. The receiver signal (a) B-type steel-UHPC and (b) C-type steel-NSC

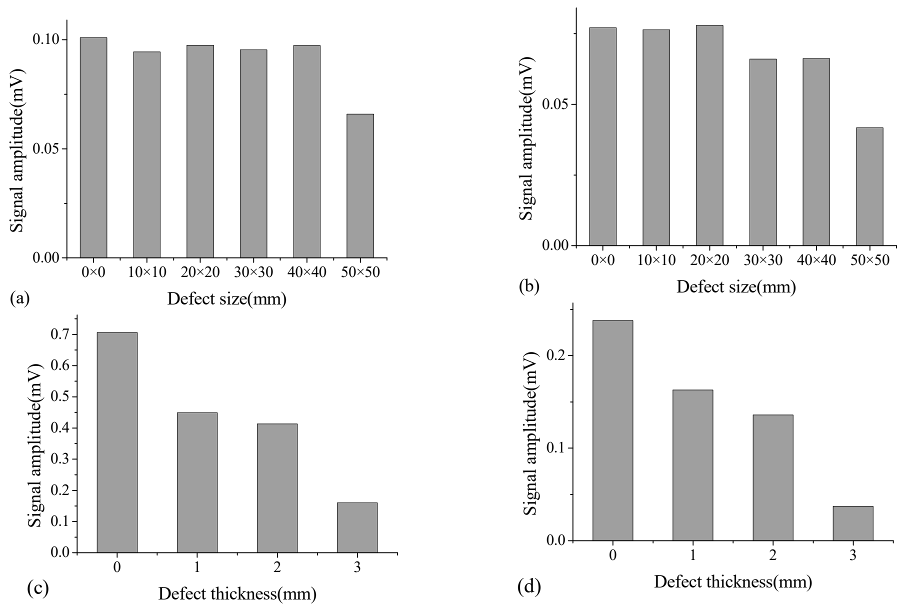

Figure 9. The amplitude values of the receiver signal at A-type plates (a) 10kHz excitation voltage frequency; (b) 15kHz excitation voltage frequency. The amplitude values of the receiver signal at B-type plates (c) 10kHz excitation voltage frequency; and (d) 15kHz excitation voltage frequency.

3.2.4. Signal amplitude

Figures 9 (a) and (b) show the amplitude values of the receiver signal at A-type plates at two frequency values of 10 kHz and 15kHz, respectively. The amplitude change is insignificant as the debonding area increases. When the debonding area reaches 50mm × 50mm, the amplitude decreases dramatically, indicating that the effect of the debonding area on the wave propagation signal is

Preprints (www.preprints.org) | NOT PEER-REVIEWED | Posted: 30 April 2018 doi:10.20944/preprints201804.0386.v1

limited. Therefore, the damage area is preset to 50mm × 50mm for the B-type composite plate. The effect of debonding thickness on the detection accuracy is investigated at this preset condition. The amplitude values of the receiver signal at B-type plates under two frequency values of 10 kHz and 15kHz are indicated in Figures 9(c) and 9(d). As indicated, the amplitude of the receiver signal decreases gradually as the debonding thickness increases. However, at the frequency of 10kHz, the amplitude difference between the receiver signals is not significant when the debonding thickness values are 1mm and 2mm, respectively.

4. PSO-k-means clustering based debonding detection

4.1 PSO-k-means clustering algorithm

This paper proposes an innovative debonding detection method based on the improved PSO (Particle Swarm Optimization) - K-means clustering algorithms [22,23]. The proposed method integrates the global searching ability of PSO method and the quick convergence characteristic of K-means clustering. The global search ability of the PSO algorithm is enhanced by dynamically tuning the inertia weights of the particles. The particles zoning is determined by the nearest neighbor approach. The post convergence of the particles is accelerated through the quick searching of the K-means clustering approach. The fitness variance threshold and the maximum number of iterations are used to determine the iterative execution. The ideal clusters are obtained from the global searching of the optimal clusters in particles. The number of clusters k = 4 and the number of particles n = 10 are taken. The particles are firstly initialized through randomly assigning a data sample as the initial cluster, i.e., initializing the optimal position. The procedure is repeated for n times. The clusters zoning is determined by the nearest-neighbors method. Given a data sample set X_i, if

$$\left\|X_i - C_j\right\| = \min\left\|X_i - C_i\right\|, (i = 1, 2..., k), \tag{2}$$

Then X_i belongs to cluster j. The parameter C_i is the jth cluster. Given a particle, the fitness F_i is the sum of the distance between sample in the cluster and the clustering center, i.e.,

$$F_i = \sum_{i=1}^{L}\sum_{j=1}^{k}\left\|X_i - C_j\right\|^2, \tag{3}$$

where L is the number of the clustering samples. After the initial clustering, the speed and location of particles are updated according to the learning factor and inertia weight coefficients. With the initial speed of zero, we have

$$V_i^{t+1} = \omega V_i^t + c_1 r_1 (P_i^t - X_i^t) + c_2 r_2 (P_g^t - X_i^t), \tag{4}$$

$$X_i^{t+1} = X_i^t + V_i^t, \tag{5}$$

where V_i^t is the speed of particles; X_i^t is the location of particles (i = 1, 2 ,…, N, in which N is the dimension of space); P_i^t is the optimal position of particles; P_g^t is the global optimal value; r_1 and r_2 are random values in [0, 1]; c_1 and c_2 are learning factors; and w is the inertia weight, which is modified dynamically within the whole iterative process. In general, the larger inertia weight indicates the better global searching capability, while the smaller inertia weight indicates the better local searching capability. The linear iteration strategy is taken in this study with the preset maximum iteration number. The inertia weight is updated as follows

$$\omega = \omega_{\max} - iter \times \frac{\omega_{\max} - \omega_{\min}}{iter\max}, \tag{6}$$

where *iter* is the current iteration and w_{max} = 0.9 and w_{min} = 0.4 are the maximum and minimum iterations, respectively. Through dynamically updating the inertia weight, the proposed algorithm can provide the better global searching ability in the early iteration, while the better local searching ability in the latter. The clusters are re-calculated after the updating of the velocity and position. The fitness values of individual and global particles are also updated to the optimum.

4.2 Features and samples selection

As described previously, the impedance curves and receiver signals are obtained at the debonding status with different thickness from impedance and wave propagation methods, respectively. The obtained curves and signals contain the features representing the damage status at different degrees. The proposed clustering algorithm is then applied to obtain the clusters representing different damage status. Mathematically, the cluster centre is the shortest distance from each point in the cluster to the centre. For a new test, the Mahalanobis distance is calculated for each testing data to the cluster centre. The testing data is then classified into the clusters with the shortest distance, which can be used to identify the damage status and damage severity. The cluster centres comprehensively integrate different features obtained from impedance-based and wave propagation methods, thus reducing the probability of false identification. Table 4 shows the 4 extracted features sensitive to different damage severity. Through repeating the tests, 50 samples are obtained from the damage status at the debonding interface with 4 different thickness values, yielding 200 samples. Each sample contains 4 features.

Table 4. Extracted features within this study

Item	Features	Source
1	RMSD(6000~8000kHz)	Impedance method
2	RMSD(10000~12000kHz)	Impedance method
3	Signal amplitude（10kHz）	Wave Propagation method
4	Signal amplitude（15kHz）	Wave Propagation method

The selected features, number of samples and quality of samples play an important role on the detection accuracy. As the number of features and samples increase or the quality enhances, the cluster centres will be optimized continually, leading to more accurate detection results. In this study, effects of different features and various numbers of samples for clustering on the detection result are investigated. Table 5 shows the cases investigated in this study. Different ratios of samples are randomly selected as clusters learning and the rest is used as testing of detection. Figure 10 shows the optimal fitness curves obtained from the clustering for the debonding interface at 4 different thickness values for cases 10-12. It is observed that, as the iteration increases, the fitness of particles decreases, indicating the improved clustering results.

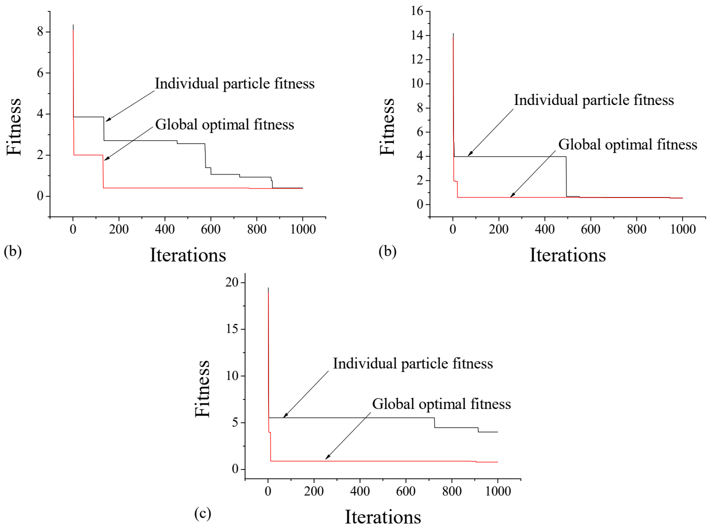

Figure 10. Fitness curves of particles (a) case 10; (b) case 11; and (c) case 12

 doi:10.20944/preprints201804.0386.v1

Table 5. Cases setting investigated in this study

Item	Selected features	Samples for clustering /(proportion)	Samples to be detected
1	1,2	60（30%）	140
2	1,2	100（50%）	100
3	1,2	140（70%）	60
4	1,3	60（30%）	140
5	1,3	100（50%）	100
6	1,3	140（70%）	60
7	3,4	60（30%）	140
8	3,4	100（50%）	100
9	3,4	140（70%）	60
10	1,2,3,4	60（30%）	140
11	1,2,3,4	100（50%）	100
12	1,2,3,4	140（70%）	60

4.3 Debonding identify using mahalanobis distance

The Mahalanobis distance of each sample data to the cluster center is calculated for 4 different debonding status. The sample data is classified into the cluster with the minimum Mahalanobis distance, thus obtaining the damage status [24]. Figure 11 shows the detection results for 4 different features. As indicated, debonding status at 0 mm and 3mm thickness can be effectively detected and the proposed method is able to effectively detect the healthy and most damaged status. Due to the limited number of samples for clustering, the features have similar values for the debonding thickness at 1mm and 2mm. In general, the probability of detection increases as the number of samples increases, indicating the detection accuracy is improved as the increase of the clustering samples.

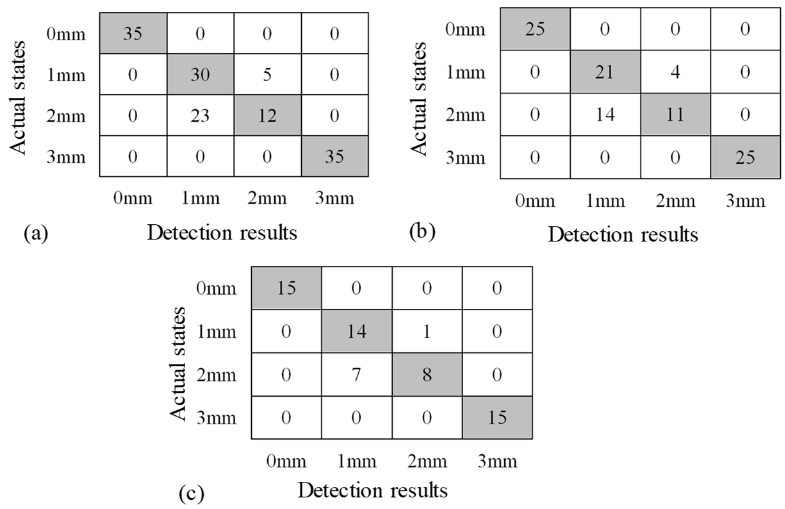

Figure 11. Detection results (a) case 10; (b) case 11; and (c) case 12.

For the same features and sampling proportion in the aforementioned cases, the detection results rely on the quality of clustering learning sample as well. The sample quality is investigated by recalculating 100 times for each case. Figure 12 shows the calculation process. When the sample quality is poor, the cluster centers at the debonding status of 1mm and 2mm is very close, resulting in high false detection and low probability of detection. When the sample quality is good, the probability of detection reaches up to 90%.

 doi:10.20944/preprints201804.0386.v1

In general, the more samples and the better quality of the samples for modeling, the higher probability of detection. In comparison to the number of samples, the quality plays more significant role on the detection accuracy. The detection result also relies on the selected features as indicated in Table 6. When both features 1 and 2 from the impedance method are selected, the expected probability of detection is 62.1% - 67.8%. When feature 1 from the impedance method and feature 3 from wave propagation method are selected, the expected probability of detection is 71.2% - 73.6%. When both features 3 and 4 from the wave propagation method are selected, the averaged probability of detection reaches to 77.5% - 83.5%. The wave propagation method can provide a better detection result than those from the impedance method. When all four features are selected, the averaged probability of detection reaches to 78.5% - 86.3%.

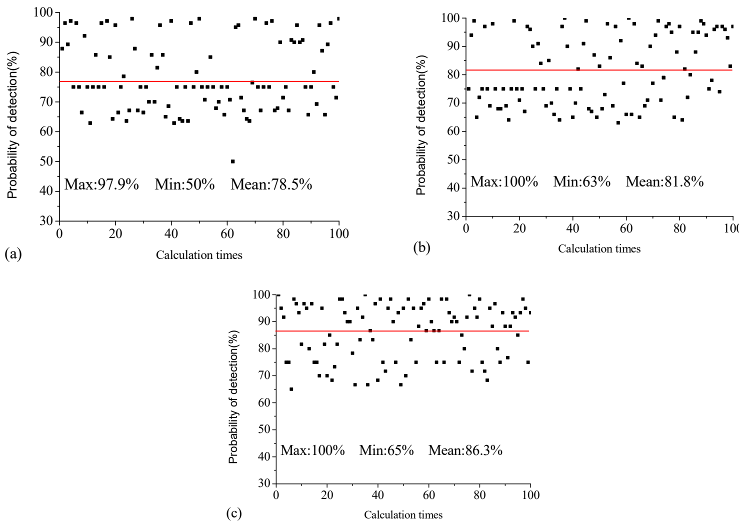

Figure 12. Probability of detection (a) case 10; (b) case 11; and (c) case 12.

Table 6. The averaged probability of detection under different cases

Cases	Selected features	Proportion of the samples for clustering		
		30%	50%	70%
1~3	1,2	62.1%	64.7%	67.8%
4~6	1,3	71.2%	71.5%	73.6%
7~9	3,4	77.8%	81.1%	83.5%
10~12	1,2,3,4	78.5%	81.8%	86.3%

5. Conclusions

This paper investigates the effectiveness of the impedance-based PZT method for debonding detection of steel-UHPC composite structure. The effects of several influencing factors, including the sensitive frequency range, PZT sensor position, and UHPC and NSC materials, on the detection accuracy are investigated. It is observed that at the higher frequency range (6000 - 12000 kHz), the separation is significant for different PZT impedance curves with various local damage levels. The closer the PZT sensor position to the damage location, the more significant separation is observed. The RMSD is employed as an evaluation indicator of debonding damage degree. Accordingly, the change of RMSD value is not sufficient when the debonding area or the thickness of steel-UHPC interface is smaller. When the debonding area of steel-UHPC interface reaches to over 30mm × 30mm, or the thickness is above 2mm, the RMSD provides an effective tool to detect the debonding damage.

This paper also investigates the effectiveness of the wave propagation-based PZT method for debonding detection of steel-UHPC composite structure. Similar to the impedance method, the effect of several influencing factors, including the excitation signal frequency, signal amplitude, and different signal transmission media (UHPC and NSC), on the detection accuracy is investigated. At the frequency range of 5 - 15 kHz for the excitation signal, the change of the receiver signal amplitude can indicate the damage degree. For the case with the smaller debonding area, the change of receiver signal amplitude is not significant. However, when the debonding area reaches up to over 50mm × 50mm, the amplitude degrades significantly. For the damage cases with different thickness values, the debonding damage can be qualitatively identified through the change of receiver signal amplitude. When the debonding thickness is over 3mm, the damage can be quantitatively detected.

This paper further develops the PSO-K-means clustering algorithm to improve the debonding detection accuracy by using the features extracted from both the impedance and wave-propagation methods. Two features, RMSD and receiver signal amplitude obtained from the impedance and wave-propagation methods, are used in the investigation. Furthermore, the effect of several influencing factors on the probability of detection is assessed. It is observed that more samples with better quality can result in the higher probability of detection. The debonding damage is sensitive to the receiver signal amplitude extracted from the wave propagation method, which indicates the better quality. The quality of samples plays a more significant role on the probability of detection.

Author Contributions: Conceptualization, Banfu Yan. and Xudong Shao; Methodology, Qiqi Zou and You Dong; Validation, Banfu Yan, Qiqi Zou and You Dong; Formal Analysis, Qiqi Zou and You Dong; Writing-Original Draft Preparation, Banfu Yan; Writing-Review & Editing, You Dong.

Funding: This research was funded by National Natural Science Foundation of China (Grand No. 51578227), the Major Program of Science and Technology of Hunan Province (Grand No. 2017SK1010), and The Hong Kong Polytechnic University under Start-Up Fund (1-ZE7Q)

Conflicts of Interest: The authors declare no conflict of interest. The founding sponsors had no role in the design of the study; in the collection, analyses, or interpretation of data; in the writing of the manuscript, and in the decision to publish the results".

References

1. AFGC, Ultra high performance fibre-reinforced concretes **2013**, AFGC Publication, Pairs, France, 2013.
2. X.D. Shao, D.T. Yi, Z.Y. Huang, H. Zhao, B, Chen, M.L. Liu, Basic Performance of the Composite Deck System Composed of Orthotropic Steel Deck and Ultrathin RPC Layer, J. Bridge Eng **2013**, 18(5), 417-428.
3. S.H. Zhang, X.D. Shao, J.H. Cao, J.F. Cui, J.H. Hu, L. Deng, Fatigue performance of a lightweight composite bridge deck with open ribs, J. Bridge Eng. **2016**, 21(7), 04016039.
4. Y. Dong, Performance assessment and design of Ultra-High Performance Concrete (UHPC) structures incorporating life-cycle cost and environmental impacts, Construction & Building Materials, **2018**, 167, 414-425.
5. J.W. Ayresy, F. Lalande, Z. Chaudhry, C.A. Rogers, Qualitative impedance-based health monitoring of civil infrastructures, Smart Mater. Struct. **1998**, 7, 599-605.
6. S.Park, PZT-based active damage detection techniques for steel bridge components, Smart Mater. Struct. **2006**, 15, 957-966.
7. F.P. Sun, Z. Chaudhry, C. Liang, C.A. Rogers, Truss structure integrity identification using PZT sensor-actuator, J. Intell. Mater. Syst. Struct. **1995**, 6, 134-139.
8. C. Liang, F.P. Sun, C.A. Rogers, Coupled electromechanical analysis of adaptive material systems-determination of the actuator power consumption and system energy transfer. J. Intell. Mater. Syst. Struct. **1994**, 5, 12-20.
9. Y. Yang, C.K. Soh, J. Xu, An integrated evolutionary programming and impedance-based NDE method, Proceedings of SPIE-The International Society for optical Engineering, San Diego; **2000**, pp. 154-161.
10. T. Coverley, W.J. Staszewski, Impact damage location in composite structures using optimized sensor triangulation procedure, Smart Mater. Struct. **2003**, 12(5), 795-803.
11. C.G. Karayannis, C.E. Chalioris, G.M. Angeli, N.A. Papadopoulos, M.J. Favvata, C.P. Providakis, Experimental damage evaluation of reinforced concrete steel bars using piezoelectric sensors, Constr. Build. Mater. **2016**, 105, 227–244.
12. D.Y. Xu, X. Cheng, S.F. Huang, M.H. Jiang, Identifying technology for structural damage based on the impedance analysis of piezoelectric sensor, Constr. Build. Mater. **2010**, 24, 2522-2527.

 doi:10.20944/preprints201804.0386.v1

13. E. Sevillano, R. Sun, A. Gil, R. Perera, Interfacial crack-induced debonding identification in FRP-strengthened RC beams from PZT signatures using hierarchical clustering analysis, Compos. Part B. **2016**, 87, 322-335.
14. Y.B. Liang, D.S. Li, S.M. Parvasi, Q.Z. Kong, I. Lim, G.B. Song, Bond-slip detection of concrete-encased composite structure using electro-mechanical impedance technique, Smart Mater. Struct. **2016**, 25 (9), 095003.
15. C.S. Wang, F.K. Chang, Built-in diagnostics for impact damage identification of composite structures, Proc.3rd Int. Workshop on Structural Health Monitoring, Stanford, USA; **1999**, pp. 612-621.
16. Y.S. Roh, F.K. Chang, Built in diagnostics for identifying an anomaly in plates using wave scattering, Stanford University, California; **1999**.
17. C.S. Wang, Structural health monitoring from fiber-reinforced composites to steel-reinforced concrete, Smart Mater. Struct. 2001, 10(3)(2001)548-552.
18. G. Song, H. Gu, Y.L. Mo, T.T.C. Hsu, H. Dhonde, Concrete structural health monitoring using embedded piezoceramic transducers, Smart Mater. Struct. **2007**, 16(4), 959-968.
19. Y.Y. Lim, K.Z. Kwong, W.Y.H. Liew, C.K. Soh, Practical issues related to the application of piezoelectric based wave propagation technique in monitoring of concrete curing, Constr. Build. Mater. **2017**, 152, 506-519.
20. Y. Lu, J.C. Li, L. Ye, D. Wang, Guided waves for damage detection in rebar-reinforced concrete beams, Constr. Build. Mater. **2013**, 47, 370-378.
21. B. Xu, T. Zhang, G.B. Song, H.C. Gu, Active interface debonding detection of a concrete-filled steel tube with piezoelectric technologies using wavelet packet analysis, Mech. Syst. Signal Process. **2013**, 36, 7-17.
22. C.Y. Tsai, I.W. Kao, Particle swarm optimization with selective particle regeneration for data clustering, Expert Systems with Applications **2011**, 38, 6565–6576.
23. T. Niknam, B. Amiri, An efficient hybrid approach based on PSO, ACO and K-means for cluster analysis, Appl. Soft Comput. **2010**, 10, 183-97.
24. S.M. Xiang, F.P. Nie, C.S. Zhang, Learning a Mahalanobis distance metric for data clustering and classification, Pattern Recognition **2008**, 41, 3600-3612.